One-dimensional scanning of moisture in porous materials with NMR

K. Kopinga
Department of Physics, Eindhoven University of Technology, P.O. Box 513, 5600 MB Eindhoven, The Netherlands

L. Pel
Department of Architecture and Building Technology (FAGO), Eindhoven University of Technology, P.O. Box 513, 5600 MB Eindhoven, The Netherlands

(Received 14 September 1993; accepted for publication 25 August 1994)

A versatile and modular nuclear magnetic resonance (NMR) instrument is described that is particularly suited for the study of moisture transport in porous media such as various building materials in which moisture can give rise to several kinds of damages. Quantitative measurements of one-dimensional moisture profiles and their time evolution can be performed on cylindrical samples having a diameter up to 20 mm with a spatial resolution better than 1 mm. Water absorption and drying experiments on various building materials demonstrate that the instrument can also be used for materials containing relatively large amounts of magnetic impurities, which until now were hardly accessible by NMR techniques. © *1994 American Institute of Physics.*

I. INTRODUCTION

Research on dynamic moisture transport in porous media is an area of continuing research in various disciplines, e.g., chemical engineering, civil engineering, and soil science. An example is formed by various building materials, such as fired-clay brick and gypsum, where the presence of moisture may give rise to frost damage, salt crystallization, and mould growth. The basic equations for moisture transport in porous materials were first established by Philip and de Vries.[1] In recent years, a more fundamental basis is given for these equations by Withaker[2] and Bear.[3]

If one uses the description given by Philip and de Vries, a major problem is the experimental determination of the various coefficients in their equations. Often overall techniques are used which only give the average moisture content as a function of time (e.g., drying curve). To derive the diffusion coefficient from such experiments one is forced to assume a relation between this coefficient and the actual moisture content that cannot be verified experimentally. Hence, it is very advantageous to measure the moisture profiles as a function of time, since in that case the diffusion coefficient can be determined directly.

The moisture transport in soils is generally studied by fast neutron thermalization methods,[4] using down-hole *in situ* probes. In civil and chemical engineering, where the processes of interest involve substantially smaller geometrical and time scales, the classical way to obtain moisture concentration profiles is the gravimetric method. Although this is the most direct method to determine an overall moisture content, it has two major disadvantages regarding moisture concentration profiles. First, it is a destructive method and therefore every profile has to be determined using different samples. The fact that one is not always able to exactly duplicate sample preparation and experimental history obscures the interpretation of the data. Apart from this, the method is laborious and time consuming. Second, the method is not accurate in its spatial resolution. Slices that can be cut are of the order of 0.5 to 1 cm, depending on the type of material. The moisture content that is determined is the average over such a slice. Especially steep gradients, which occur, for example, in the case of a receding drying front, cannot be determined by this method.

An experimental method to determine transient moisture concentration profiles should therefore preferably be nondestructive and give a high spatial resolution. Examples of these methods are gamma[5] or neutron[6] attenuation, and nuclear magnetic resonance[7] (NMR). Of these methods NMR offers the best sensitivity, as it is directly related to the amount of hydrogen nuclei, unlike the attenuation methods. With NMR, also a distinction can be made between free, physically bound, and chemically bound water.

In an NMR experiment, the magnetic moments of the hydrogen nuclei are manipulated by suitably chosen rf fields, resulting in a so-called spin-echo signal, which contains information about the magnetic fields acting on these nuclei and their local environment.[8] This information is lost if the time scale of a single spin-echo experiment exceeds the so-called transverse relaxation time (T_2) of the nuclei. Usually, in porous materials T_2 is dominated by surface relaxation processes and diffusion. In inorganic building materials like brick and mortar, however, large amounts of paramagnetic ions (e.g., Fe) are present, which cause T_2 to decrease dramatically. Apart from this, due to the difference of the magnetic susceptibility of water and the porous material, local field gradients will be induced, which broaden the resonance lines and thereby limit the spatial resolution. These properties present special demands on the strategy of the measurements and the hardware performance.

The transverse relaxation times of the hydrogen nuclei are often very small (<200 μs), an hence the duration of the radio frequency (rf) pulses should preferably not exceed a few tens of microseconds. To achieve a spatial resolution in the order of 1 mm, magnetic field gradients of about 40 Gs/cm (0.4 T/m) are required. Since our primary goal is the investigation of one-dimensional moisture profiles, both static and dynamic, we have not attempted to switch the field gradients during the individual pulse sequences, i.e., within 20 μs. The spin-echo signal was excited by using straight-

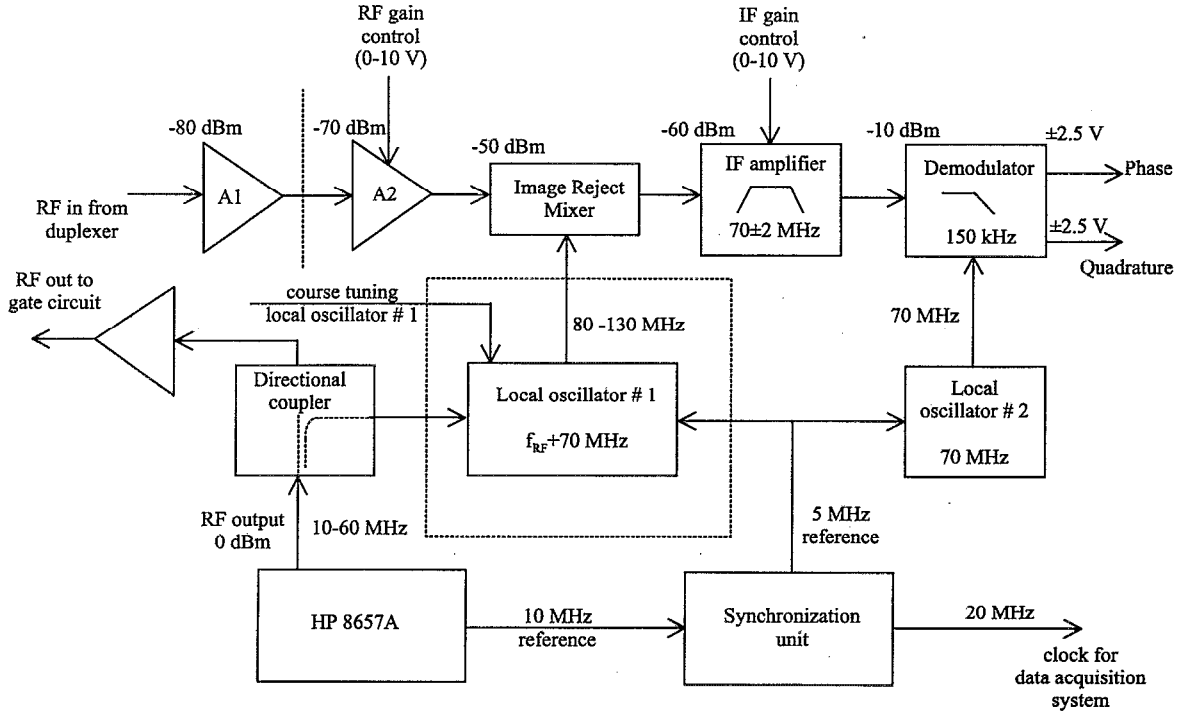

FIG. 1. Schematic diagram of the rf receiver section. In this section, the rf spin-echo signal is amplified, demodulated, and filtered. The resulting phase and quadrature output signals are fed to the analog-to-digital converters of the data-acquisition system. The section also supplies a 20 MHz master clock for this system and generates the rf input signal for the gate circuit of the power transmitter. The local oscillator 1 is plotted in more detail in Fig. 2.

forward Hahn sequences at a fixed strength of the magnetic field gradient. The slice selection was achieved by adjusting the rf carrier frequency or by positioning the sample with a translator, controlled by a step motor.

Since the time scale of the experiments covers the region from a few seconds to a few days the measurements are fully automated. The scanning of a moisture profile and its time dependence over the sample requires a strong interaction between the settings of the rf system, magnetic field gradient, sample positioning, and sample conditioning. To achieve the necessary flexibility we developed a fully modular rf system of which all relevant settings can be controlled by a general purpose data acquisition system, described in the next section. In Sec. III, we will discuss some details of the experimental setup, including the rf probe head, whereas in Sec. IV the performance of our equipment will be evaluated and illustrated with some representative experimental results.

II. RADIO FREQUENCY SECTION AND DATA ACQUISITION

Except for a linear 100 W rf power amplifier and a HP 8657A frequency synthesizer, the entire rf section is built up from small circuit blocks, which are commercially available (Mini-Circuits,[9] ANZAC,[10] Synergy[11]). In Fig. 1, a schematic diagram of the receiver is shown. This receiver covers the rf range from 10 to 60 MHz, corresponding to experiments in magnetic fields between 0.25 and 1.5 T. All relevant settings (gain, phase, local oscillator frequency) can be controlled by applying dc voltages in the range 0–10 V to the corresponding inputs. These voltages are supplied by a 12 bit, 8 channel DAC in our data-acquisition system. The video output voltages appearing at the outputs P and Q are in the range −2.5 to +2.5 V, suitable for most fast ADCs.

The spin-echo signal present at the input is first amplified by A_1. For this section, we used a circuit block type CDM23, manufactured by ADE,[12] which has a gain of 9 dB and a noise figure $F=1$ dB in the frequency range of interest, and is located close to the LC circuit containing the sample (see Sec. III). Next, the signal is amplified by section A_2, consisting of a 28 dB amplifier (MCL MAN-1LN), a voltage controlled attenuator (MCL PAS-1), an 18 dB amplifier (MCL MAN-2), and a 3 dB fixed attenuator. The latter attenuator is inserted to rule out instabilities due to impedance mismatch between the various sections. Section A_2 offers a gain between 0 and 40 dB, which can be controlled by a dc voltage between 0 and 10 V. Next, the signal is fed into an image reject mixer (Synergy IMP 972), where it is mixed with a local oscillator signal in the frequency range 80–130 MHz. The difference signal $f_{LO1}-f_{rf}$ is processed by an intermediate frequency (if) amplifier with a pass band of 70±2 MHz and a gain between 10 and 55 dB, controlled by a dc voltage between 0 and 10 V. The intermediate frequency is chosen above the rf range for two reasons. First, the local oscillator signal for the image reject mixer covers a frequency range of less than a factor 2, and hence can be excited by a single oscillator circuit. Second, a flat frequency response within several MHz can rather easily be achieved using conventional coupled LC circuits. The if section consists of a pre-filter, built up from a constant impedance 70 MHz bandpass filter (MCL PIF-70), a high dynamic range 10

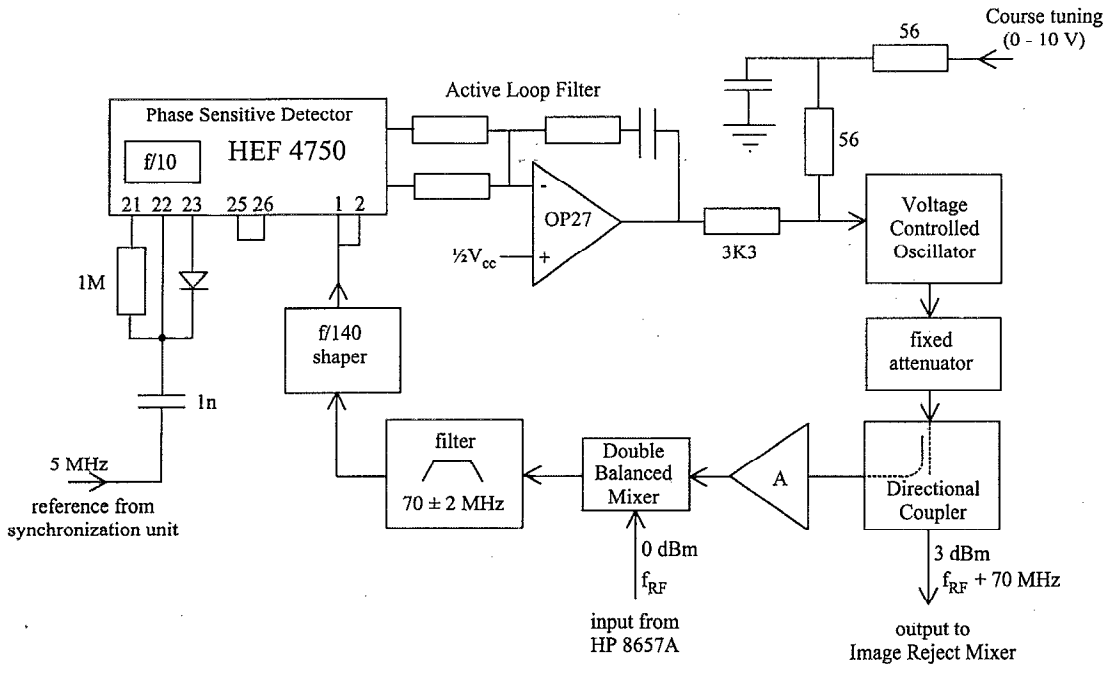

FIG. 2. Schematic diagram of the local oscillator 1. This circuit generates a signal at a frequency exactly 70 MHz above the frequency of the signal used to excite the spin-echo. Synchronization of the various signals is maintained by the 5 MHz signal derived from the reference output of the HP 8657 A frequency synthesizer (cf. Fig. 1).

dB amplifier (MCL MAN-1HLN), again a MCL PIF-70 filter, and the actual tuned amplifier. This amplifier is built up from, successively, a coupled pair of LC circuits ($Q=6$), a high dynamic range 10 dB amplifier (MCL MAN-1HLN), a coupled pair of LC circuits, a 16 dB amplifier (MCL MAN-1AD), a voltage controlled attenuator (MCL PAS-1), a 28 dB amplifier with a noise figure below 3 dB (MCL MAN-1LN), a coupled pair of LC circuits, and a 16 dB amplifier (MCL MAN-1AD). To eliminate possible instabilities of the amplifier blocks, due to the large impedance mismatch of the LC circuits outside the pass band, the input and output of each pair of coupled LC circuits are connected via 3 dB fixed attenuators (MCL AT-3). Measurements on the if section revealed that the frequency response was flat within 0.1 dB within the pass band 70 ± 2 MHz. Apart from this, the recovery time from severe overload conditions (10 dBm input signals) did amount to less than 1 μs.

The output signal of the if section is fed into a demodulator, consisting of a power splitter (MCL PSC-2-1W) and two identical stages for the in-phase and quadrature signals, respectively. Each stage contains a high dynamic range 10 dB amplifier (MCL MAN-1HLN), a double balanced mixer (DBM) (MCL SRA-1MH), and a video amplifier. The local oscillator (LO) signals for the two mixers are supplied by a 70 MHz oscillator. The output of this oscillator is connected to a 90° hybrid (Synergy DQP 256) and the resulting signals are amplified by MCL MAN1-HLN circuit blocks to a level of about 13 dBm. The video amplifiers consist of an active second-order low-pass Bessel filter with a -6 dB cutoff frequency of 150 kHz, incorporating an Analog Devices AD841[13] operational amplifier, followed by an output stage with a voltage gain of 40, incorporating an AD840 opamp. The circuit can drive up to ±2.5 V into a 50 Ω load.

All oscillator frequencies used in the receiver are phase-locked to the 10 MHz reference output of the HP 8657A frequency synthesizer, which acts as a master oscillator. For this purpose, the reference output is connected to a phase-locked loop (PLL) which contains a 40 MHz voltage controlled oscillator (VCO). From this oscillator a symmetrical 20 MHz TTL compatible output signal is derived, which is used as a clock signal for the interfaces of our data-acquisition system. By further frequency division an internal 5 MHz signal is obtained, to which the local oscillators are phase locked.

The circuit diagram of one these oscillators (1) is plotted schematically in Fig. 2. The VCO is a commercially available circuit block (ADE VCO 80-160) yielding an output power of approximately 12 dBm with very low phase noise. Via a fixed 5 dB attenuator (MCL AT-5) and a directional coupler (MCL PDC-20-1W) a small fraction (-25 dB) of the output power of the VCO is fed into an amplifier section (A) consisting of a fixed 5 dB attenuator, an 18 dB amplifier (MCL MAN-2), and a high dynamic range 10 dB amplifier (MCL MAN-1HLN). The resulting $+10$ dBm signal serves as LO signal for a double balanced mixer (DBM) (MCL SRA-1MH). A fraction of the 0 dBm rf output signal of the HP 8657A synthesizer is connected to the rf input of this DBM via a directional coupler (MCL PDC-20-1W) and an 18 dB amplifier (MCL MAN-2). The directional couplers and subsequent amplifiers were found to provide sufficient isolation between the synthesizer and the VCO. The output signal of the DBM is led through two constant impedance filters (MCL PIF-70) with a center frequency of 70 MHz to suppress spurious signals, which may hamper correct opera-

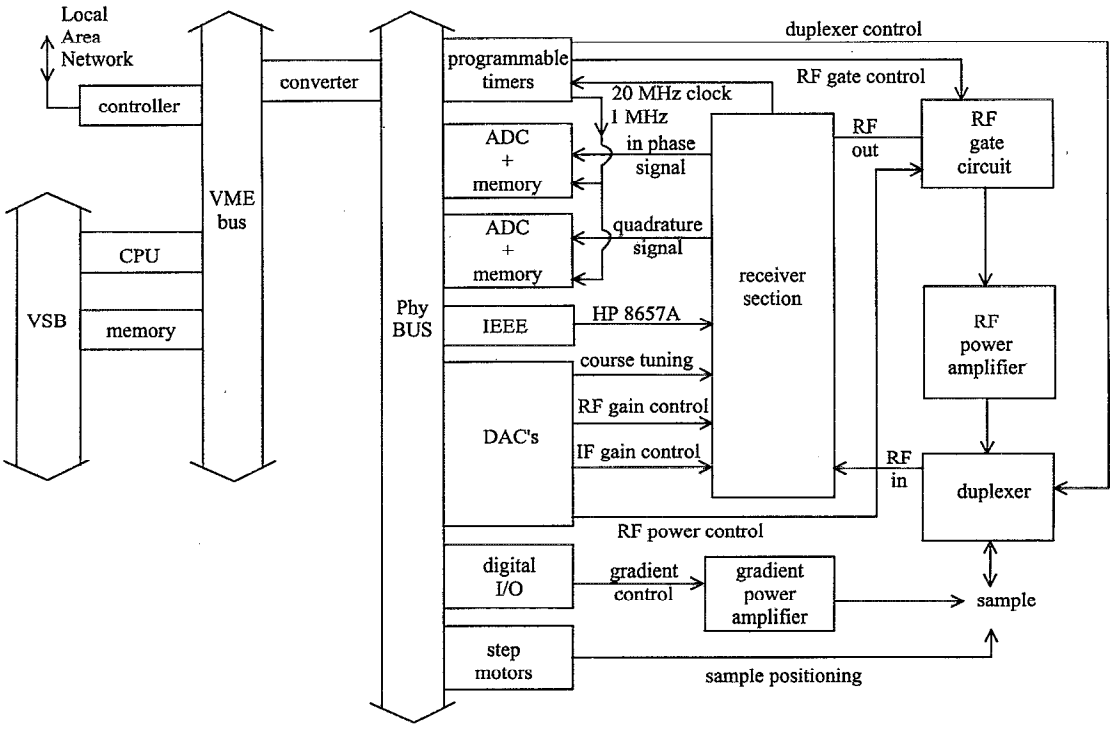

FIG. 3. Block diagram of the data-acquisition system and the rf receiver/transmitter sections. The receiver section is shown in more detail in Fig. 1.

tion of the phase detector. Next, the signal is converted into a digital signal by a pulse shaper, the frequency is divided by a factor of 140, and the resulting 500 kHz signal is connected to one of the inputs of the phase sensitive detector (PSD) (Philips HEF 4750[14]). The other input section of this PSD is connected to the 5 MHz reference signal mentioned above, of which the frequency is divided by a factor of 10 in the PSD itself. Phase comparison therefore occurs at a frequency of 500 kHz. The HEF 4750 was chosen because of its very low phase noise and low spurii. Apart from this, the gain of the phase detector of this device in locked condition is very high (typically 1 kV/rad) and hence the noise contribution from the active loop filter (OP27) can be neglected. Because of the presence of the 70 MHz bandpass filter at the output of the DBM, the VCO has to be set to within 2 MHz from the desired frequency (f_{rf}+70 MHz) before the PLL will operate correctly. Therefore, the output of the loop filter is connected to the control input of the VCO via a 30:1 attenuator, whereas a dc voltage in the range 0 to 10 V is applied to a coarse tuning input. The phase locked loop of the local oscillator module 2 is largely identical to that of module 1, except for the amplifier section A and the DBM, which are omitted, whereas a voltage controlled phase shifter (Synergy PP-904) is placed at the output.

The phase noise introduced by these local oscillators was found to be very low: measurements in which the output of the HP synthesizer was connected to the receiver input via a 40 dB attenuator revealed a phase noise of the P,Q output voltage vector of less than 1 deg over the entire rf range. By changing the rf and if gain settings, input signals in the range −100 dBm to −20 dBm could be handled without complications. The recovery time of the complete receiver chain after a +10 dBm input signal was found to be less than 5 μs, which is much smaller than the time between the second rf pulse of the Hahn sequence used to excite the spin-echo and the start of the spin-echo signal itself (>20 μs).

The transmitter section consists of a gate circuit and a 100 W linear rf power amplifier. As input signal for the gate circuit the 0 dBm rf output signal of the HP 8657A synthesizer is used, which is first led through a directional coupler (see Fig. 1), a fixed 3 dB attenuator (MCL AT-3), and a MCL MAN1-HLN 10 dB amplifier. The rf gates are identical to that described in Ref. 15, except that fixed 3 dB attenuators (MCL AT-3) have been included at the input and output to reduce the impedance mismatch and spurious harmonic contents of the output signal. One of the double balanced mixers (MCL SRA-1H) in the first gate is switched with either a positive or a negative current, thus providing a zero or 180° phase shift of the rf output signal. By using two rf gates, which are fairly well isolated from each other, we obtained an on–off ratio exceeding 100 dB.

To connect the LC probe circuit to either the transmitter or the receiver section, a duplexer is used that incorporates series-parallel switches of 500 V PIN diodes (MA4P506[16]). These diodes are biased with 70 mA in forward direction (r_s~0.3 Ω) or with −60 V in reverse direction (c_j=0.7 pF) by complementary pairs of fast switching transistors. The duplexer is switched about 500 ns before and after the rf gate circuit is activated, using a TTL compatible logic signal supplied by our timer interface.

Our data-acquisition system, which is schematically plotted in Fig. 3, is controlled by a processor module (M68030 CPU and M68882 coprocessor) that is intercon-

nected with a 16 Mbyte global memory module via an industry standard VME/VSB bus system. Via the VME bus the CPU communicates with a local area network controller and a so-called VME/PhyBUS converter. The latter offers a transparent coupling (including DMA facilities) between the VME bus and a user defined bus (PhyBUS), which accommodates the various interfaces, that will now briefly be discussed.

Via a 12 bit 8 channel DAC a voltage in the range 0 to 10 V can be applied to the control inputs GC-rf, GC-if, CT-LO1, and φ of the receiver section (see Figs. 1 and 2) as well as the rf power control input of the transmitter driver. Two channels of the step motor interface are connected directly to the drivers of the step motors used for sample positioning. One of the channels of the logic (0–5 V) input/output system is used to activate a power Mosfet circuit that switches the current through the field gradient coils. As was already mentioned in the introduction, the magnetic field gradient is kept at a constant (preset) value during the individual pulse sequences. During the time intervals between adjacent sequences the current through the coils is switched off to avoid excessive heating.

The industry standard IEEE interface communicates directly with the HP–IB interface of the HP 8657A synthesizer. Apart from the initialization routine, this communication is mainly used to set or change the frequency during the scans of the moisture profile. The timer section has several functions. First, it performs a frequency division of the 20 MHz master clock signal, providing a 1 MHz trigger signal for the ADCs connected to the P and Q output of the receiver. Second, it contains several programmable timers/preset scalers which are used to generate the 90°/180° rf pulses (see Sec. III), the switching signal for the multiplexer, and a gate signal for the ADC triggers. All timing signals are synchronized to the 20 MHz clock; they can be adjusted with a resolution of 50 ns.

The P and Q signals are digitized by a 12 bit ADCs at a rate of 1 MHz, which exceeds the cutoff frequency of the Bessel filters in the video output stages by more than a factor of 6. The resulting digital values are stored as 16 bit numbers in successive locations of 2 Mbyte dual ported static memory modules with auto-increment address registers. The ADCs are triggered only during the time interval that the spin-echo occurs, i.e., for a period of 512 μs after the second rf pulse. After a number of spin-echo signals have been collected, the contents of the memory modules are transferred to VME memory for further processing.

III. EXPERIMENTAL SETUP

The samples used in our experiments are cylindrical rods with a diameter of 20 mm and a length varying between 2 and 20 cm. They can be inserted in a cylindrical coil with an inner diameter of 35 mm, made of 7 turns of 1 mm Cu wire. This coil forms part of a tuned LC circuit and is placed within a shielded box. Since our aim is to perform quantitative measurements of the moisture profile, the LC circuit has to be carefully matched to the characteristic impedance of our equipment (50 Ω), whereas changes in the rf losses or detuning of the circuit due to variations of the moisture content of the sample should be as small as possible. To reduce the effect of variations of the dielectric permittivity of the sample, a cylindrical Faraday shield has been placed between the coil and the sample. This shield consists of 0.5 mm insulated Cu wires running parallel to the axial direction of the coil. The wires are electrically interconnected and grounded at the lower side of the shield. A small slit in this part of the shield prevents the generation of Eddy currents and consequent rf power losses.

The coil is part of a series tuned circuit, shown in the inset of Fig. 4. Impedance matching is achieved by adjusting the capacitor C_p. To minimize detuning by the presence of a sample the quality factor Q of the circuit has been reduced to $Q \sim 40$ by adding a series resistor r_s. At this moment the equipment is operated at frequencies near 33 MHz, corresponding to an applied field of 0.78 T. This field was chosen as a compromise between the signal-to-noise ratio of the spin-echo signal, which increases at higher frequencies, and the line broadening due to the presence of magnetic impurities, which leads to a decrease of the resolution at higher magnetic fields. The magnet is a conventional water cooled, iron cored, electromagnet. The poles of this magnet have a diameter of 20 cm and are 5 cm apart. The magnetic field has a stability better then 5×10^{-5} T/week and a homogeneity of 4×10^{-5} T over 1 cm dsv.

A magnetic field gradient is generated in the vertical direction by a set of conventional Anderson coils.[17] As already mentioned in the introduction, gradients of 0.25 to 0.5 T/m are needed to achieve a spatial resolution better than 1 mm. The coils were found to provide a field gradient which was constant within 1% over 30 mm in the vertical direction. Using the LC circuit described above, a 90° turning angle of the ^{1}H spins can be achieved with pulses having a duration of 15 μs, corresponding to an rf magnetic field amplitude $B_1 \simeq 0.4$ mT. Because of the large field gradient, a measurement of the spin-echo signal and subsequent Fourier transformation yields a moisture distribution within a vertical region of only 2 to 3 mm. To determine the moisture profile over a larger region, the sample can be moved in the vertical direction by a translator driven by a step motor. In some experiments, however, where the temperature, air flow, and relative humidity have to be controlled, it is preferable to measure the moisture profile without moving the sample. This can be realized by changing the rf center frequency f_c; for a typical magnitude of the field gradient a frequency shift of 100 kHz corresponds to a shift of the selected region of 7 mm. These kinds of experiments are performed without retuning the LC circuit, since that would give rise to an unacceptable low speed of the measurements.

In Fig. 5, we have reproduced the results of such an experiment on a homogeneous reference sample, i.e., a quartz tube filled with 0.1 M solution of $CuSO_4$ in water. The Fourier transformed spin-echo signals at various rf center frequencies are denoted by curves, each reflecting the region selected at that particular value of f_c. The set of solid curves is called a reference profile. Inspection of the figure reveals that the maximum observed spin-echo intensity decreases when the frequency f_c is shifted away from the value f_0 corresponding to the center of the coil. This decrease, de-

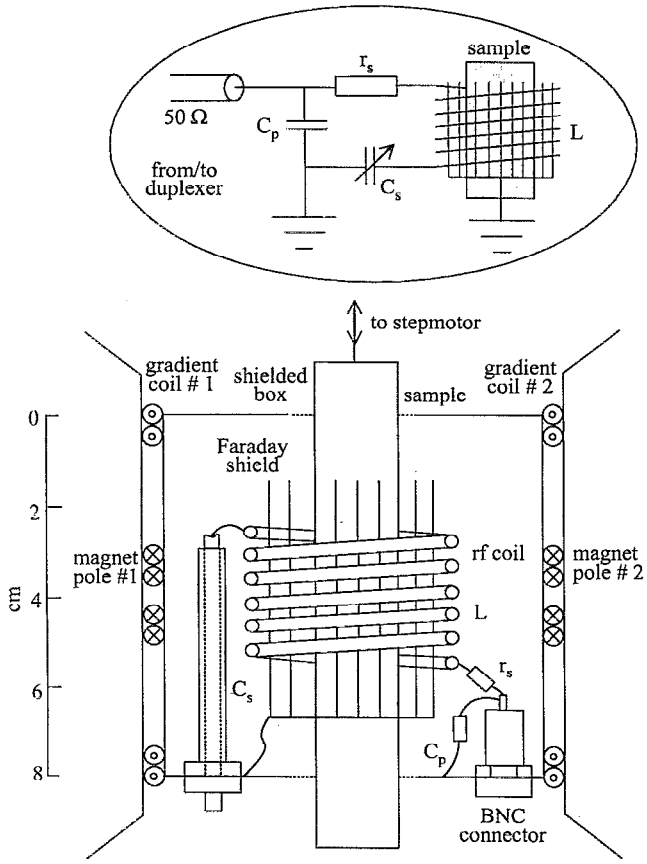

FIG. 4. Schematic diagram of the rf probe head that accommodates the sample. The homogeneous magnetic field B_0 points in the horizontal direction, whereas the two gradient coils generate a magnetic field gradient in the vertical direction. The inset shows the electronic equivalent circuit.

noted by the "envelope" of the curves (dashed curve in Fig. 5), is a largely geometrical effect, resulting from the finite length of the rf coil. This was checked by decreasing the magnitude of the field gradient by a factor of 2, which did hardly affect the envelope of the curves (in spatial coordinates), although the corresponding frequency shifts decrease by the same factor. In this respect, we like to note that the quality factor of our LC circuit ($Q \sim 40$) has only a small effect on the shape of the curves presented in Fig. 5, since it causes a decrease of sensitivity by 3 dB for a frequency shift of at least 400 kHz.

An actual moisture profile is determined by measuring the spin-echo signal of the sample of interest at a number of frequencies, that exactly match the frequencies f_c at which the reference profile has been determined. The signal detected at each frequency is Fourier transformed and the result $I(f_c, f-f_c)$ is divided by the intensity of the corresponding points of the reference profile. In this way the geometrical effect is eliminated, as was checked by measurements on various phantom samples. The results of this point by point division at various values of f_c are combined to obtain the overall moisture profile over about 25 mm. In this process only the data around the maximum of each curve at fixed f_c are taken, since they have the best signal to noise ratio. Generally, measurements on fully saturated samples are used to calibrate our apparatus for a certain sample material, which enables us to determine the corresponding moisture profiles with an absolute accuracy of a few percent.

IV. TYPICAL PERFORMANCE

The one-dimensional spatial resolution of our equipment was evaluated by measurements on cylindrical samples with a flat top or bottom. The moisture profile near the flat surface of such samples was obtained following the procedure sketched in Sec. III, and is presented in Fig. 6 for various materials. For a phantom sample containing 0.1 M solution of $CuSO_4$ in water the resolution amounts to about 0.8 mm, whereas for both porous materials the resolution is found to decrease by 10%–20%. This is attributed to the presence of inhomogeneously distributed para- or ferromagnetic impurities in these materials, which induce local random magnetic fields and hence a significant line broadening. The longitudinal and transverse relaxation times (T_1 respectively T_2) for these samples were determined by varying the timing of the pulse sequence, and are summarized in Table I. Resolution profiles like those presented in Fig. 6 can, in principle, be used to correct the measured moisture profiles using a suitable deconvolution procedure. However, since in our current investigations a spatial resolution of 1 mm is sufficient, no such attempts were made.

Next, the absolute accuracy of our equipment was tested by measurements on various series of representative samples with a different moisture content, that was determined independently by the gravimetric method. In Fig. 7, we have plotted the integrated moisture profile obtained from NMR

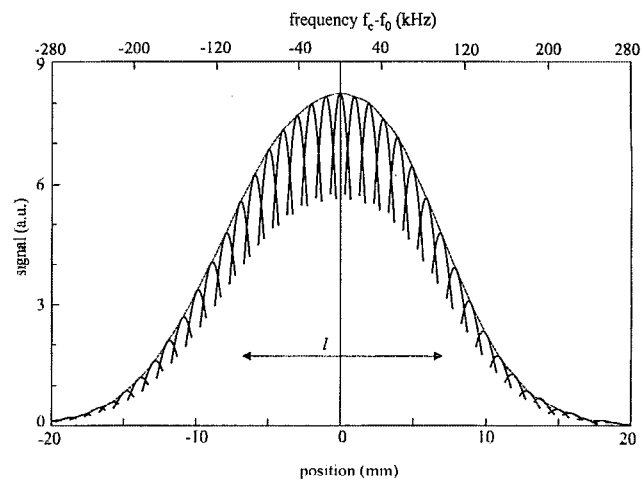

FIG. 5. Typical reference profile obtained from a sample with a homogeneous moisture distribution. Solid curves represent the Fourier transforms $I(f_c, f-f_c)$ of the spin-echo signals detected at a series of rf center frequencies f_c. Because of the presence of a magnetic field gradient, each of these curves reflects a slice of the sample selected at that particular value of f_c. Only the parts of these curves with the largest contribution to the signal are plotted. The dashed curve (a kind of "envelope") reflects the effect of the finite length (l) of the rf coil, which gives rise to a decreasing sensitivity as the selected slice moves away from the centre of the coil. The total set of the solid curves is used as a reference profile. The horizontal arrow marked l denotes the region occupied by the coil of the rf probe during a drying experiment.

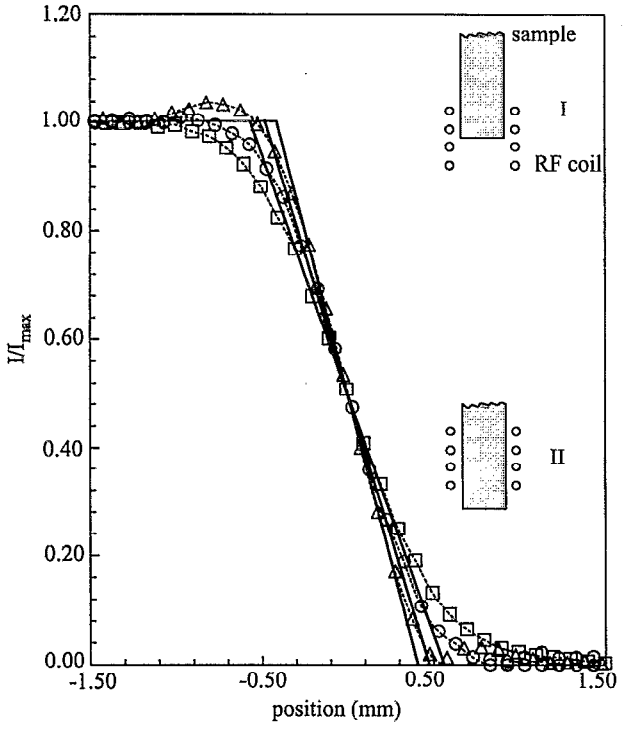

FIG. 6. One-dimensional spatial resolution for several materials: (△) 0.1 M $CuSO_4$ solution, (○) lime–sandstone, (□) red brick. The inset of the figure illustrates how this resolution has been determined. First, a raw profile is measured using a cylindrical sample of which the flat top or bottom is positioned near the center of the rf probe head (I). Next, the reference profile of the sample is measured by positioning the homogeneous region of the sample in the probe head (II). Finally, a point-by-point division of the two profiles is performed.

experiments against the mass of water for two series of samples. The corresponding plots show a perfect linear behavior. The scatter of the data is comparable to the observed signal to noise ratio (~2%). It appears that the samples of machine moulded fired clay red brick [made from a clay with high Fe content (~4%), hence the red color] produce a substantially smaller NMR signal than the samples of lime sandstone, and also have a smaller value of T_2 (see Table I). Both effects can be explained by the relatively large amount of Fe present in the former material. Obviously, the NMR signal is strongly dependent of the type of material and therefore results like those presented in Fig. 7 are used to convert observed moisture profiles into absolute values.

From series of measurements performed with our equipment on a variety of building materials, it appeared that the sample of red brick had the lowest signal to noise ratio. To our knowledge, no NMR experiments on this type of material have been reported, in contrast to, e.g., sandstone and limestone which have S/N ratio's that are higher by almost one order of magnitude and values of T_1 and T_2 that allow more or less standard 2D imaging experiments.[18–21] To illustrate the potential capabilities of our equipment, we will therefore discuss the results of both an absorption and a drying experiment on a sample of red brick.

In Fig. 8, we have plotted the raw data obtained from the absorption experiment. The figure shows a number of partial profiles, each corresponding to 7 data points around the rf

TABLE I. Spin-lattice (or longitudinal) relaxation time T_1 and spin-spin (or transverse) relaxation time T_2 for several materials. T_1 sets a lower limit to the time duration between subsequent pulse sequences. T_2 effectively sets an upper limit to the time duration between the pulses within 1 Hahn sequence and hence the spin-echo acquisition time.

Material	T_1 (ms)	T_2 (μs)
0.1 M $CuSO_4$	<10[a]	4600
Lime–sandstone	45	850
Brick red[b]	300	200
Brick yellow[c]	350	750

[a]Cannot be measured with our pulse sequence.
[b]Made from a clay with a high Fe content (~4%), hence the red color.
[c]Made from a clay with a low Fe content (<0.1%), hence the yellow color.

center frequency f_c ($=f_0$ in this experiment) (see Fig. 5). Each partial profile was acquired in 12 s. Since, especially just after the start of the experiment, the velocity of the wetting front may be rather high, a time stamp is added to each set of points to allow a meaningful interpretation of observed profiles in terms of appropriate theoretical models.[22] In this experiment, the sample was moved in the vertical direction by means of the translator. The entire experiment took about 1 h. We like to note that in this experiment the time resolution was limited by the relatively poor S/N ratio of the red

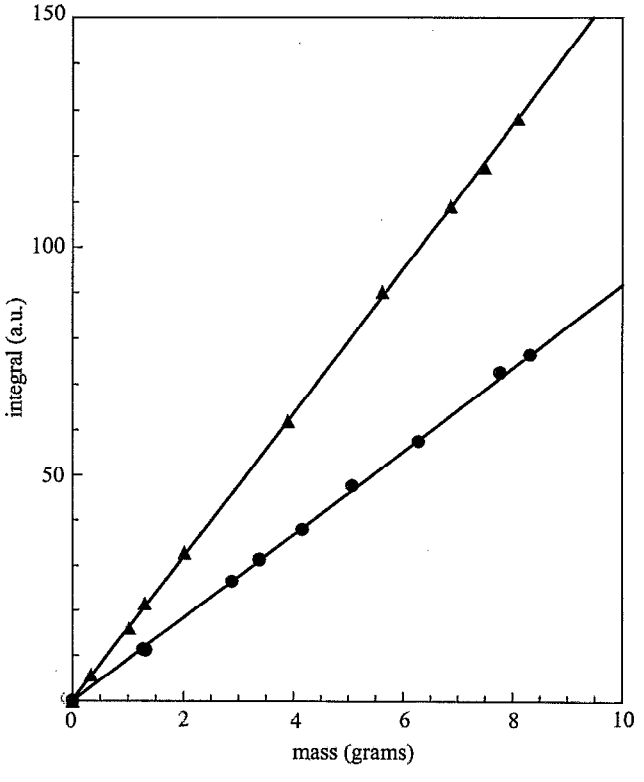

FIG. 7. Calibration of the NMR signal: (▲) lime–sandstone, (●) red brick. For different values of the moisture content, the moisture profile of a sample of a certain material is determined by NMR measurements, and is integrated over the entire sample. The resulting values of the integral are given along the vertical axis. The corresponding masses of water present in the sample during these measurements are determined by gravimetric methods and are given along the horizontal axis. From the slope of the straight line describing the data for a certain sample, an absolute calibration of the NMR signal for that sample (or that material) can be obtained.

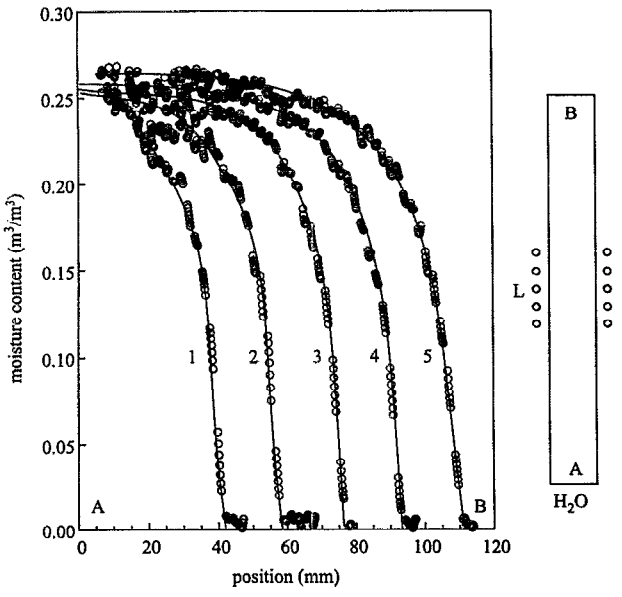

FIG. 8. The raw data collected during an absorption experiment. In this kind of experiment, the lower side of the sample (position A in the figure) is immersed in water. The frequency is fixed at the value f_0 corresponding to the centre of the rf coil (see Fig. 5.) Hence, only the moisture distribution in a small region of the sample is measured simultaneously (in this case, seven closely spaced points). After determination of such a partial profile, the sample is translated by a step motor over a few mm. This is repeated until, for instance, a complete wetting front in the sample [solid curve (1) in the figure] has been measured. After some time, during which the wetting front has moved through the sample, the entire procedure is repeated, now yielding the new wetting front (2), and so on.

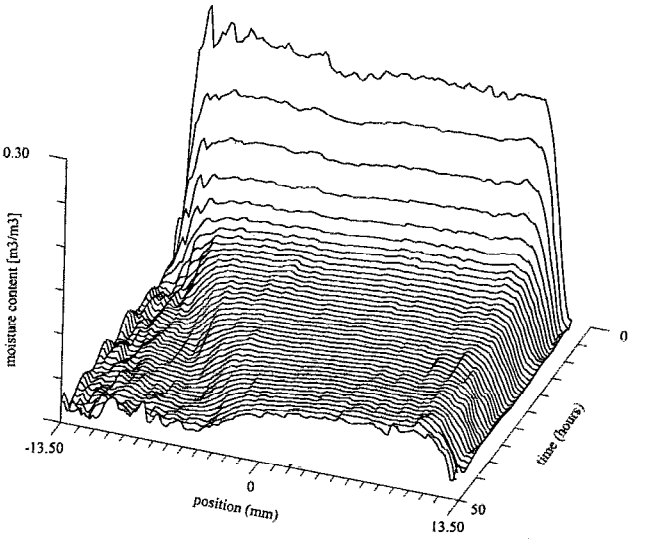

FIG. 9. Moisture concentration profiles of red brick during drying. In this kind of experiment a completely wetted sample, with a length of 25 mm, is isolated with Teflon (PTFE), except for one side. In practice, this is the upper side; in the figure, it corresponds to a position of −12.50 mm. Drying is achieved by a controlled air flow. By using a relatively long rf coil (l) and varying the frequency f_c (see Fig. 5), the entire sample region can be scanned. The resulting moisture profiles, corresponding to time intervals of 1 h, are represented by solid curves. In this case, the individual profiles show fluctuations that exceed the experimental noise by a factor of 5. These fluctuations reproduce from curve to curve, and reflect inhomogeneities of the sample.

brick samples. In materials like sandstone, limestone, and lime–sandstone, a complete steep wetting front can be measured in about 10 s.

The moisture profiles in the drying experiment were collected every hour. In this case, the acquisition of a single profile (150 pixels) with a signal to noise ratio of about 50 took about 40 min. By interpolating data corresponding to the same spatial coordinate, profiles were constructed that represent the actual moisture distribution at well defined moments in time. Such profiles are plotted in Fig. 9. The time evolution of the drying front is observed very clearly. Especially the horizontal part of the profiles shows some fluctuations that should be attributed to inhomogeneities of the sample rather than experimental noise. A detailed interpretation of these measurements is beyond the scope of this paper, and will be published elsewhere.

In view of the results presented in this section, we conclude that the NMR equipment described in this paper offers the possibility to determine the time evolution of one dimensional moisture profiles in a large variety of porous materials, including those containing relatively large amounts of magnetic impurities, with a spatial resolution of 1 mm and an absolute accuracy of a few percent. Of course, the performance can be improved by increasing the power of the rf pulses, thereby selecting a larger sample region at one time, or by increasing the magnitude of the field gradient, yielding an increase of the 1D resolution. The effect of such modifications is currently being studied.

ACKNOWLEDGMENTS

The authors wish to thank H. P. Otten, J. Noijen, and A. P. de Boer for their indispensable help in building and operating the NMR equipment. We also like to thank the group Physical Instrumentation for their help. This project was financially supported by the Royal Association of Dutch Brick Manufacturers (KNB).

[1] J. R. Philip and D. A. de Vries, Trans. Am. Geophys. Un. **38**, 222 (1957).
[2] S. Withaker, Adv. Heat Transfer **13**, 119 (1977).
[3] J. Bear and Y. Bachmat, *Introduction to Modelling of Transport Phenomena in Porous Media*, Vol. 4 (Kluwer, Dordrecht, 1990).
[4] Neutron Moisture Gauges, Technical reports series 112, International Atomic Energy Agency, Vienna (1970).
[5] J. M. Davidson, J. W. Biggar, and D. R. Nielsen, J. Geophys. Res. **68**, 4777 (1963).
[6] L. Pel, A. A. J. Ketelaars, O. C. G. Adan, and A. A. van Well, Int. J. Heat Mass Transfer **36**, 1261 (1993).
[7] R. J. Gummerson, C. Hall, W. D. Hoff, R. Hawkes, G. N. Holland, and W. S. Moore, Nature **281**, 56 (1979).
[8] R. L. Dixon and K. E. Ekstrand, Med. Phys. **9**, 807 (1982).
[9] Mini-Circuits, P.O. Box 350166, Brooklyn, NY 11235.
[10] ANZAC, 80 Cambridge Street, Burlington, MA 01803.
[11] Synergy Microwave Corporation, 483 Mc. Lean Boulevard, Paterson, NJ 07504.
[12] Avance et Développement Electronique (ADE), 2 bis, rue Léon Blum -Z.I.- 91120 Palaiseau, France.
[13] Analog Devices, One Technology Way, P.O. Box 9106, Norwood, MA 02062.
[14] Philips Components Division, Strategic Accounts and International Sales, P.O. Box 218, 5600 MD Eindhoven, The Netherlands.

[15] T. Claiborne, J. T. Cheng, A. R. Garber, and P. D. Ellis, Rev. Sci. Instrum. **58**, 742 (1987).
[16] M/A-COM Silicon Products Inc., One South Avenue, Burlington, MA 01803.
[17] W. A. Anderson, Rev. Sci. Instrum. **32**, 241 (1961).
[18] T. A. Carpenter, E. S. Davies, C. Hall, L. D. Hall, W. D. Hoff, and M. A. Wilson, Mater. Struct. **26**, 286 (1993).
[19] G. Guillot, A. Trokiner, L. Darrasse, and H. Saint-Jalmes, J. Phys. D **22**, 1646 (1989).
[20] E. J. Fordham, T. P. L. Roberts, T. A. Carpenter, and L. D. Hall, AIChE J. **37**, 1895 (1991).
[21] P. A. Osment, K. J. Packer, M. J. Taylor, J. J. Attard, T. A. Carpenter, L. D. Hall, N. J. Herrod, and S. J. Doran, Philos. Trans. R. Soc. London Sect. A **333**, 441 (1990).
[22] C. Hall, Building Envir. **16**, 117 (1977).